Ballistic hot-electron transistors

by M. Heiblum M. V. Fischetti

We present an overview of work at the IBM Thomas J. Watson Research Center on the tunneling hot-electron transfer amplifier (THETA) device-including its use as an amplifier and as a tool for investigating ballistic hot-electron transport. In the initial, vertically configured version of the device, a quasi-monoenergetic, variable-energy, hot-electron beam is generated (via tunneling) which traverses a thin GaAs region and is then collected and energyanalyzed. As the hot electrons traverse the device, they are used to probe scattering events, band nonparabolicity, size-quantization effects, and intervalley transfer. A recent, lateral version of the device has been used to demonstrate the existence of ballistic hotelectron transport in the plane of a twodimensional electron gas, and the associated possibility of achieving high gain.

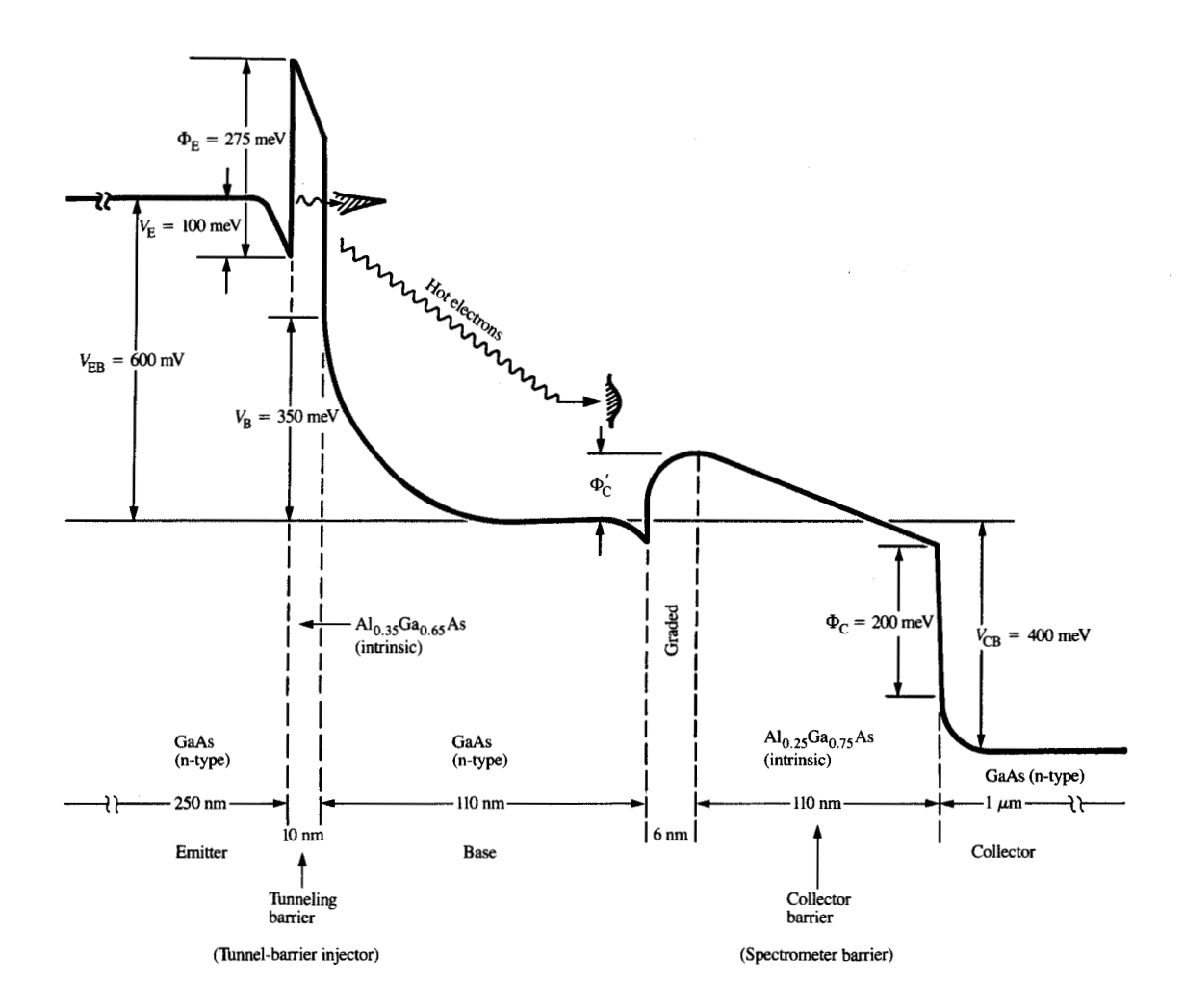
Introduction

In a perfectly periodic crystal, free electrons are expected to move smoothly without colliding with the crystal atoms, at a velocity determined by the crystal structure. The free electrons are regarded as traveling ballistically.

[®]Copyright 1990 by International Business Machines Corporation. Copying in printed form for private use is permitted without payment of royalty provided that (1) each reproduction is done without alteration and (2) the *Journal* reference and IBM copyright notice are included on the first page. The title and abstract, but no other portions, of this paper may be copied or distributed royalty free without further permission by computer-based and other information-service systems. Permission to *republish* any other portion of this paper must be obtained from the Editor.

However, in reality, phonons are emitted by the electrons, even at 0 K, causing scattering. In addition, in a real crystal, other mechanisms influence the free electron motion, leading to a mean free time between collisions, an average electron group velocity, and a mean free path (MFP—the mean free time between collisions times the average electron group velocity). If the MFP is of the same order of magnitude as the length of the sample, the total electron population can be regarded as being composed of two ensembles: a ballistic one and a quasi-ballistic one; the latter consists of those electrons which have been scattered at least once and thus have suffered energy losses and/or direction changes.

In 1979 Shur and Eastman [1] proposed that ballistic electron transport could be achieved in GaAs at low temperatures at a sample length of the order of a few hundred nm. But in subsequent current-voltage experiments, Eastman et al. [2] were unable to demonstrate unambiguously the existence of ballistic transport, because of complicated boundary conditions between the n⁺ contact and n⁻ transport regions in their samples, and because of a relatively large contactresistance contribution. In 1982 Hesto et al. [3] proposed using an electron spectroscopy technique to detect energy distributions of ballistic electrons. Employing hotelectron transistors, such a technique was later used by Hayes et al. [4], Yokoyama et al. [5], and Heiblum et al. [6]. In 1985 Yokoyama et al. [5] and Levi et al. [7] provided evidence of quasi-ballistic hot-electron transport through heavily doped GaAs layers. That was followed by a direct demonstration of ballistic electron transport, and a determination of the ballistic portion of the traversing electrons, by Heiblum et al. [8]. Using improved device



Potential distribution of a typical THETA device under forward bias. Quasi-monoenergetic hot electrons are injected at the tunneling barrier; some are scattered and arrive at the collector with decreased energies. The collector barrier, which is graded, prevents thermal electrons in the base from flowing into the collector. In the device depicted, the n-type base is doped to a level of 2×10^{17} cm⁻³; thus a relatively large emitter-base bias (injection voltage) $V_{\rm EB}$ is required in order to develop a suitable tunneling current. From [6], reproduced with permission.

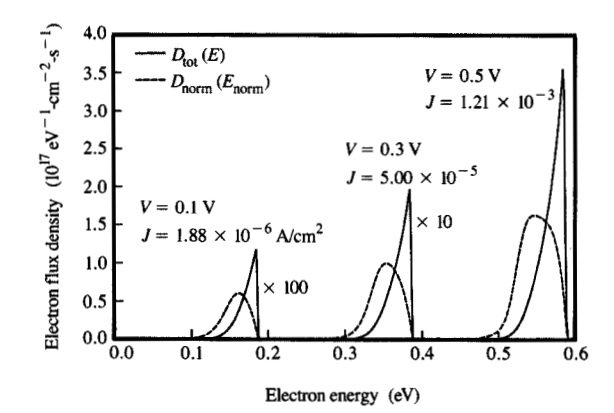
structures, ballistic portions greater than 75% were subsequently obtained [9]. Similarly, ballistic hole transport was achieved in p-type hot-electron devices; however, the ballistic portions found in those devices did not exceed about 10% [10].

Hot-electron transistors

In the hot-electron transistor, which is similar in principle to the bipolar transistor, use is made of "cold" electrons (the majority carriers, in thermal equilibrium with the lattice) and "hot" electrons (the minority carriers) rather than electrons and holes. The cold electrons provide the conductivity needed in the various

layers of the device, while the hot electrons carry the input signal that is to be amplified.

The potential distribution of a typical tunneling hotelectron transfer amplifier (THETA) device under forward bias is shown in Figure 1. Hot electrons, originating in an emitter (the cathode), are injected into a thin base (the transport region) and are collected at a collector (the anode). The base is separated from the emitter and the collector by two potential barriers that confine the equilibrium thermal electrons to their original layers. The barrier between the base and emitter (designated as the tunnel-barrier injector) is thin enough to serve as a tunneling barrier; that between the base and



Total (solid line) and normal (dashed line) calculated electron energy distributions at three different biases for a 12-nm-wide $Al_xGa_{1-x}As$ tunneling barrier, assuming x = 0.5. The magnitude of the Fermi level in the GaAs regions is assumed to be 86.4 meV.

collector (designated as the collector barrier) is thick enough to serve as an electron spectrometer barrier (discussed later). The injected hot-electron beam is energetic enough to surmount the collector barrier almost independently of the collector voltage, resulting in a high differential output resistance. It should be noted that a hot-electron device need not be a "ballistic device" to operate as a fast amplifier. If the hot electrons are injected at sufficiently high energies, they may be elastically scattered several times, undergo slight changes in their direction, and still be collected, although after a somewhat longer transit time.

◆ A brief history

The first hot-electron transistor, the cold cathode transistor, was proposed by Mead in 1960 [11]. It consisted of two metal-oxide-metal (MOM) structures in an MOMOM configuration. The first MOM portion contained a thin oxide to facilitate tunneling, and the second, a thicker oxide to prevent it. The common M layer (the base) was thin enough to allow quasi-ballistic transfer; a low base resistance was achieved because of the high conductivity of the metal layer. Since the MFP of hot electrons in metals is short, and pinhole-free thin metal layers are difficult to fabricate, the current gain of the transistor was low.

A revival of interest in hot-electron transistors started with Shannon's *camel transistor*, fabricated in 1979 using Si [12]. Subsequently, in 1980, one of us (M. Heiblum) proposed the THETA device [13]. Recently a number of hot-electron device structures have been fabricated and

tested with different degrees of success [14-21]. Here we concentrate on results obtained at the IBM Thomas J. Watson Research Center using THETA device structures.

◆ The tunnel-barrier injector

As indicated in Figure 1, in a THETA device, heterojunctions are used to form the tunneling and collector barriers. Injection of hot electrons occurs through the tunneling barrier (at the left). The barrier is thin enough to permit the flow of substantial currents when the effective barrier height for tunneling is lowered by the application of a bias $V_{\rm EB}$ between the emitter and the base. For the example depicted in the figure, the width of the injected electron energy distribution associated with electron momentum normal to the tunnel-barrier injector is about 60 meV.

The energy and angular distributions of the electrons emerging from a tunnel-barrier injector can be calculated by first solving the relevant version of the Poisson equation. A constant effective mass of $(0.067 + 0.083x)m_c$ is assumed for the electron effective mass in the AlGaAs layer, where x is the AlAs mole fraction and m_c the mass of the free electron. The tunneling current density J(V) is then obtained as a function of the applied bias V by integrating the transmission probability $T(E_\perp, V)$, where E_\perp is the energy associated with the electron momentum normal to the injector (hereafter designated as the normal energy), over the electron flux in the cathode. Using the expression

$$J(V) \simeq 2e \int \frac{d\vec{k}}{(2\pi)^3} f_{\rm C}(\vec{k}) [1 - f_{\rm A}(\vec{k})] v_{\perp}(\vec{k}) T(k_{\perp}, V), \qquad (1)$$

where $f_c(k)$ and $f_A(k)$ are the cathode and anode Fermi functions, and $v_{\perp}(E)$ is the component of the electron velocity normal to the injector, and using the relations

$$E(\hat{k}) = \frac{\hbar^2 k^2}{2m_{\rm en}(E)},\tag{2a}$$

$$\nabla_{\hat{k}} E(\hat{k}) = \frac{\hbar^2 \hat{k}}{m_{\text{out}}(E)},\tag{2b}$$

where $m_{\rm en}$ and $m_{\rm opt}$ are designated as the "energy effective mass" and the "optical effective mass," respectively [22], we can, for a spherical band, transform the integral over \hat{k} to integrals over the normal and total electron energies, namely,

$$J(V) \simeq \frac{e}{2} \int_{0}^{\infty} dE \, \frac{\rho(E) f(E) [1 - f(E + eV)]}{[2m_{\rm en}(E)E]^{1/2}} \times \int_{0}^{E} dE_{\perp} T(E_{\perp}, V).$$
 (3)

We have used only the cathode Fermi function f(E) and dropped the subscript.

Next we define the following three distributions: a total energy distribution $D_{\text{tot}}(E, V)$, a normal energy distribution $D_{\text{norm}}(E_{\perp}, V)$, and an angular distribution $D_{\text{ang}}(\theta, V)$ such that

$$J(V) = e \int_0^\infty dE D_{\text{tot}}(E, V)$$

$$= e \int_0^\infty dE_\perp D_{\text{norm}}(E_\perp, V)$$

$$= e \int_0^{\pi/2} d\theta D_{\text{ang}}(\theta, V), \tag{4}$$

In the case of parabolic bands, the three distributions reduce to

$$D_{\text{tot}}(E, V) \simeq \frac{m_{C.0}}{\pi^2 h^3} f(E) [1 - f(E + eV)] \times \int_0^E dE_{\perp} T(E_{\perp}, V),$$
 (5a)

$$D_{\text{norm}}(E_{\perp}, V) \simeq \frac{m_{C,0}}{\pi^2 \hbar^3} T(E_{\perp}, V)$$

$$\times \int_{E_{\perp}}^{\infty} dE f(E) [1 - f(E + eV)], \qquad (5b)$$

$$D_{\text{ang}}(\theta, V) \simeq \frac{2m_{C,0}}{\pi^2 h^3} \sin \theta \cos \theta$$

$$\times \int_0^\infty dE \{ E f(E) [1 - f(E + eV)]$$

$$\times T(E \cos^2 \theta, V) \}, \qquad (5c)$$

where $m_{C,0}$ is the effective mass at the bottom of the conduction band.

In Figure 2 we show the calculated total and normal energy distributions of electrons emerging from an 11.5-nm-wide, 0.53-eV-high hypothetical tunneling barrier. Figure 3 illustrates several calculated angular distributions at different biases. For most of the electrons, tunneling is expected to occur at a nonzero angle because only a vanishingly small number of them are expected to be moving in that direction. As a result, because the tunneling probability is its maximum in the normal direction, a maximum of the distribution should occur at a small but nonzero angle.

Another basic property of such a tunnel-barrier injector is its mass selectivity; the heavier the mass of a particle, the lower its tunneling probability. This property has been utilized in a p-type THETA device in which primarily light holes (LH) are injected from an emitter populated mostly with heavy holes (HH). Figure 4 shows calculated current densities due to the tunneling of holes

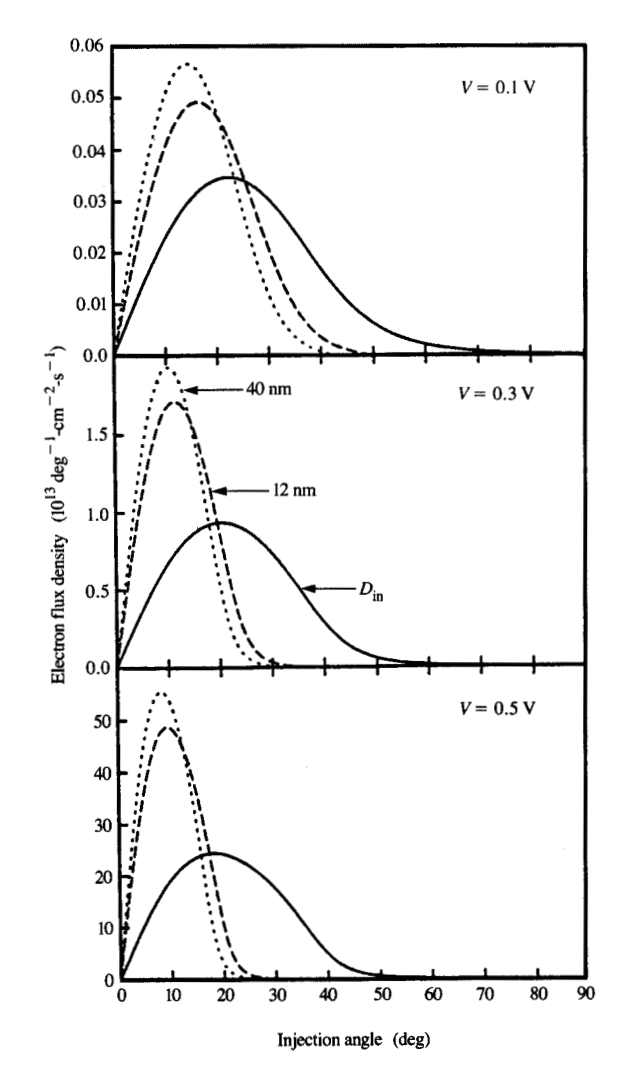
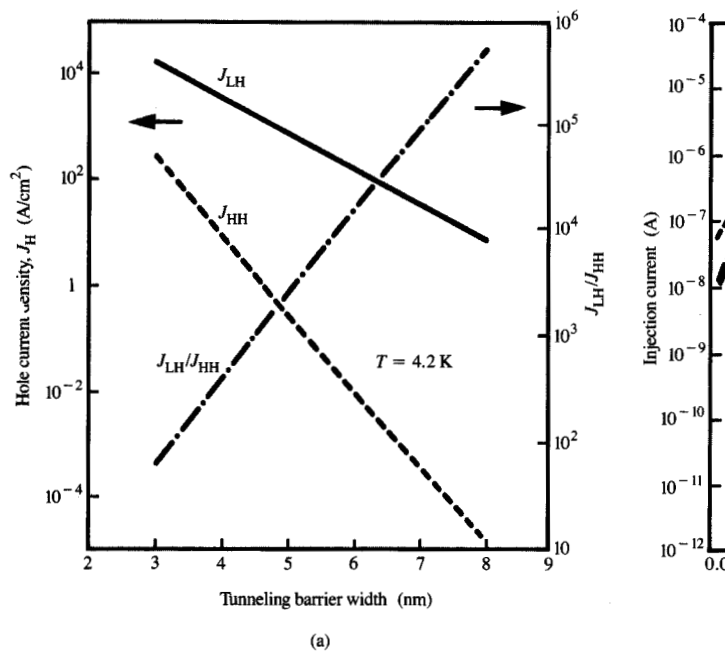
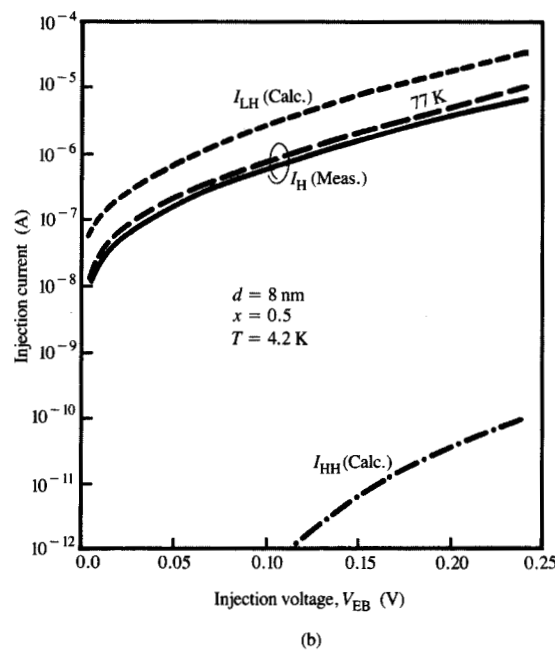


Figure 6

Calculated angular distributions of electrons tunneling through the barrier of Figure 2, at three biases. For each bias, the distributions are plotted at three positions in the device; at the cathode-AlGaAs interface $D_{\rm in}$; at a distance of 0.5 nm from the AlGaAs tunneling barrier into the anode (total distance traversed: 12 nm); and farther away in the anode (total distance traversed: 40 nm) after being subjected to the "focusing" action of the band-bending in the depleted region of the anode.

through a 0.275-eV-high AlGaAs barrier as a function of barrier thickness [part (a)], and injection current versus injection voltage [part (b)]. As can be seen, as the barrier width decreases and the current density increases, the selectivity is expected to decrease. The calculations indicate that sufficiently large current densities should be achievable if the barrier is thin, while maintaining a





(a) Calculated current density due to the tunneling of light and heavy holes through a 0.275-eV-high AlGaAs tunneling barrier, as a function of tunneling-barrier width. (b) Calculated injection current through the same barrier, as a function of injection voltage $V_{\rm EB}$; measured current $I_{\rm H}$ is also shown.

rather large selectivity ratio. Part (b) also contains a plot of measured current $I_{\rm H}$; comparison with $I_{\rm LH}$ suggests that it is due to light holes.

Energy spectroscopy

The current density J(V) at an applied voltage V can be expressed as $e \int n(E_{\perp})v_{\perp}(E) dE_{\perp}$. Although the electron energy distribution $n(E_{\perp})$ in a ballistic device is often highly nonuniform (e.g., it peaks strongly at a particular energy), its J(V) characteristics are usually monotonic and featureless. Moreover, in sufficiently narrow regions (of the order of the electron Debye length), the presence of space charge effects and the uncertainties involved in determining boundary conditions make it very difficult to identify the existence of ballistic transport from the J(V) characteristics.

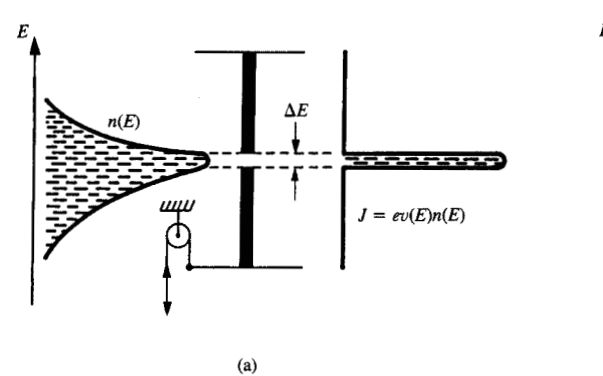
◆ High-pass spectroscopy

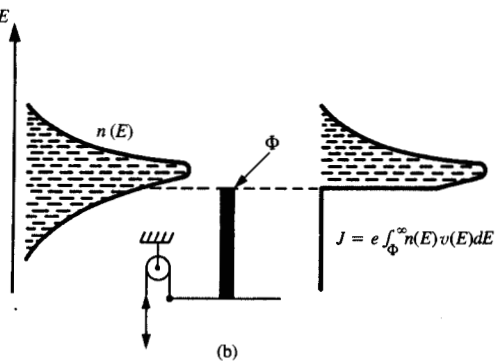
Alternatively, the use of electron energy spectroscopy to determine $n(E_{\perp})v_{\perp}(E)$, as proposed by Hesto et al. [3], is a much more effective technique for establishing the existence of ballistic transport. An ideal electron energy spectrometer should be easily calibrated, be transparent

in a defined energy "window," and be opaque outside that window.

The current density J through a narrow normal-energy window ΔE_{\perp} can be expressed as $en(E_{\perp})v_{\perp}(E)\Delta E_{\perp}$. If the indicated energy window is used to scan the energy distribution but the electron velocity is almost constant across the distribution, $J(E_1) \propto n(E_1)$, as shown in Figure 5(a). Although such a bandpass-filter spectrometer was implemented recently by Capasso et al. [23] using a double-barrier resonant tunneling GaAs-AlGaAs structure, it is difficult to calibrate and its transparency is nonconstant. A simpler and more accurate spectrometer is a high-pass-filter spectrometer, as depicted in Figure 5(a). When electrons surmount a barrier of height Φ , the resulting current density at the collector is $e \int_{\Phi}^{\infty} n(E_{\perp})v(E) dE_{\perp}$. If Φ changes by $\Delta\Phi$, the change in the measured current density is $en(E_{\perp})v_{\perp}(E)\Delta\Phi$. Thus, the normal energy distribution can be deduced from $dJ/d\Phi$ [rather than directly from J(V)], as indicated in Figure 5(b).

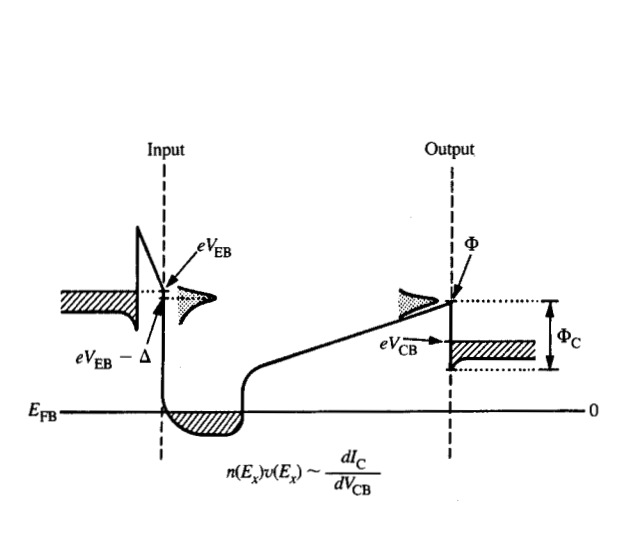
Electron energy spectroscopy in GaAs was initiated by Hayes et al. [4] and by Yokoyama et al. [5]. Here we describe the use for that purpose of THETA devices

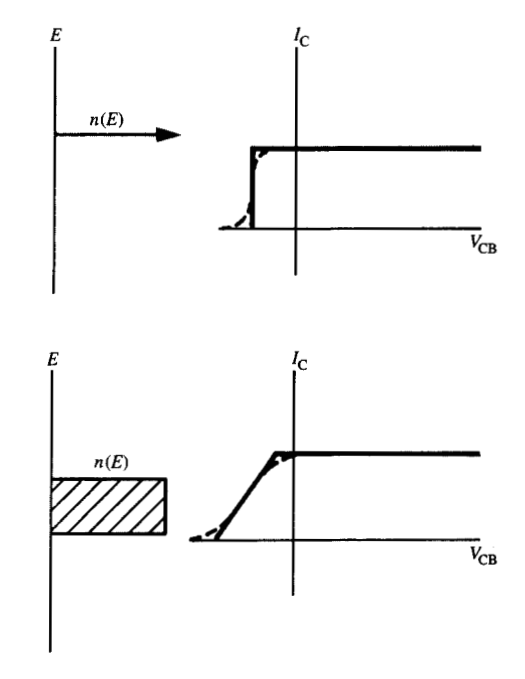




Fourters

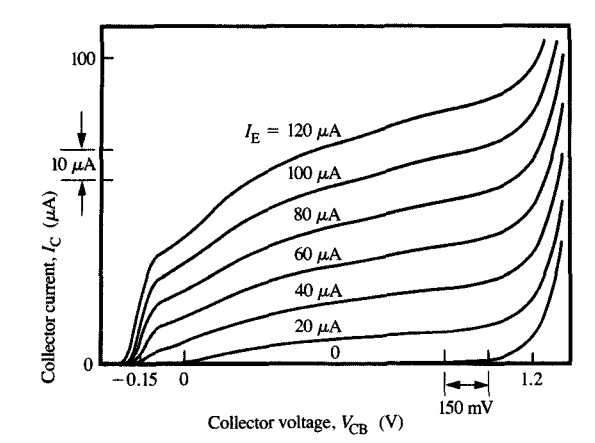
Two types of electron energy spectometers: one involves the use of a "bandpass" filter (a); the other, the use of a "high-pass" filter (b). In (a), the measured current is proportional to the energy distribution of the carriers; in (b) the derivative $dJ/d\Phi$ is proportional to that distribution. In both cases, the velocity normal to the barrier is assumed to be constant over the indicated energy range.





Energy spectroscopy by means of a THETA device. The high-pass filter is a rectangular AlGaAs collector barrier. The height of the barrier can be changed by applying a negative voltage $V_{\rm CB}$, noting that $\Delta\Phi_{\rm C}\simeq\Delta V_{\rm CB}$. Two examples of the expected dependence of $I_{\rm C}$ on $V_{\rm CB}$ are shown, one arising from a rectangular energy distribution and the other from an energy distribution characterized by a delta function.

having a rectangular collector barrier (also designated as the spectrometer barrier), as depicted in **Figure 6**. The height of the barrier can be increased by applying a negative voltage to the collector with respect to the base.



Output characteristics of a THETA device having a base width of 30 nm and a base doping level of $1 \times 10^{18} \, \mathrm{cm}^{-3}$, operated in a common base configuration, at different levels of injection current I_{E} . From [8], reproduced with permission.

The main disadvantage of such a spectrometer is that analysis is performed after the electrons traverse the total length of the barrier, thus increasing the likelihood that they will be scattered by the spectrometer.

At low temperatures, the scattering of hot electrons in undoped AlGaAs is due mainly to alloy scattering. Measurements conducted at low temperatures by Chandra and Eastman [24] on high-quality AlGaAs layers have led to an estimated alloy-scattering-dominated mobility of about 10^5 cm²/v-s and an approximate hot-electron MFP of about $0.5 \mu m$, levels which are quite suitable for purposes of spectroscopy.

Advantages of the rectangular spectrometer barrier in comparison to those produced by doping (which contain doping-related potential fluctuations) include the nearunity value of $dV/d\Phi$ (when no unintentional charges exist in the barrier) and the uniformity of its barrier height. However, even if use is made of a high-quality rectangular AlGaAs barrier, some modification of the electron distribution is induced by the barrier itself. Electrons can tunnel through the top "tip" of the barrier and also be reflected (quantum-mechanically) even if their energies extend above the barrier. The tunneling electrons therefore appear to have an elevated energy, and some broadening of the original distribution is expected. For example, for an injected energy distribution which is characterized by a delta function, we expect an apparent distribution about 8 meV wide, shifted by about 2 meV toward higher energies. Some

additional broadening is expected because of quantummechanical reflections.

Observation of quasi-ballistic and ballistic transport

Hayes et al. [4] and Yokoyama et al. [5] have published (concurrently) spectroscopic results on hot-electron transport in GaAs, verifying the occurrence of nonequilibrium, quasi-ballistic transport. In the experiments by Yokoyama et al. using the THETA device, electrons were injected into a 100-nm-wide n-type base, doped to a level of 5×10^{17} cm⁻³, and analyzed using a 150-nm-wide AlGaAs rectangular, undoped collector barrier. Relatively narrow distributions, about 150 meV wide, were measured at the collector, with an average energy loss of about 250 meV. Use was made of injection energies far in excess of the energy needed for transfer into the L valleys of GaAs. In similar subsequent experiments, Heiblum et al. [6] showed that when injection energies exceeded the Γ -L and Γ -X energy separations, all of the electrons arriving at the collectors of devices having 100-nm-wide bases were almost completely thermalized. Using devices containing barriers which were formed by planar doping, Hayes et al. [4] and Levi et al. [7] found that in devices having relatively wide bases, the arriving electrons were completely thermalized; however, when the base width was reduced to below about 85 nm, a hot-electron distribution was detected. Unfortunately, because of the poor definition of their injectors and spectrometer barriers, resulting from impurity fluctuations, they were unable to determine unequivocally the nature of the arriving electrons.

• Ballistic transport in THETA devices

Using a high-quality AlGaAs rectangular barrier as a spectrometer imbedded in a THETA device having a 30-nm-wide base doped to 1×10^{18} cm⁻³, Heiblum et al. [8] measured narrow distribution peaks. The peak of a typical distribution was close to the injection energy and was most prominent when injection energies did not significantly exceed the Γ -L energy separation (the separation between the Γ valley and the L valleys). The output characteristics of the device and the energy distributions obtained are shown in **Figures 7** and **8**. The observed distributions had a 60-meV full width at half maximum, and their peak positions shifted as the injection energy was increased.

For the "ballistic condition" to be fulfilled, the following normal energy balance equation must be satisfied:

$$eV_{EB} + \zeta - \Delta = \Phi_C + eV_{CB} \text{ (at peak)} - \delta,$$
 (6)

where $\xi = E_F - E_C$ is the energy separation between the Fermi level and the conduction-band energies, Δ is the

deviation of the normal distribution peak below the Fermi level of the emitter, δ is the band bending in the accumulation layer in the collector, $V_{\rm CB}$ (at peak) is the spectrometer (negative) applied voltage at the distribution peak, and $V_{\rm EB}$ is the injection voltage. Allowing for some uncertainties in the barrier height, it was concluded that the peak of the collected distribution could not have shifted by more than the energy of one longitudinal optical phonon (36 meV) from that of the injected distribution [8].

Increasing the base width to 72 nm resulted in the appearance of similarly peaked but smaller ballistic distributions. Defining a ballistic parameter $\alpha_{\rm B}$ by the relation $\alpha_{\rm B} \simeq I_{\rm C}(V_{\rm CB} \simeq 0)/I_{\rm E}$ (at $V_{\rm CB} = 0$ the slope of $I_{\rm C}$ is almost zero) gave measured values of $\alpha_{\rm B}$ of 0.3 and 0.15 for the devices with base widths of 30 nm and 72 nm, respectively.

A very interesting experimental observation was the preservation of the shape of the ballistic distribution. As the transport region was lengthened, more electrons were inelastically scattered out of the ballistic distribution. If small-angle scattering events had occurred, we would have expected the normal distributions to broaden (toward low energies) for longer transit distances. However, for base widths up to at least 72 nm, no change in the width of the distributions was observed!

• Observation of ballistic hole transport

The p-type THETA device is complementary to the n-type device. As already mentioned, in such a device, the tunnel-barrier injector also serves as a mass separator. The majority of holes present are heavy; only a small fraction are light (see **Figure 9**). But, as indicated by Figure 4, the injected carriers are expected to be mostly light holes. At energies close enough to the valence band, the mass of the light holes and their velocity are very close to those of the electrons. Since the heavy hole band is degenerate with the light hole band at $\vec{k} = 0$, the final density of states available for light hole scattering is very large, and the ballistic MFP of light holes is expected to be smaller than that of the ballistic electrons.

Spectroscopy performed with a p-type THETA device having a 31-nm-wide base doped to a level of 2×10^{18} cm⁻³ has indicated ballistic portions of light holes arriving at the collector as high as 8% [10]. Even when the doping was reduced to 7×10^{17} cm⁻³, the ballistic portions did not increase. It is too early at this point to speculate on the nature of the scattering mechanisms, but it is clear that they are not significantly dependent on base-layer doping level. The measured hole energy distributions were very narrow, about 35 meV wide, with a peak that changed with injection energy (**Figure 10**). The narrow width of the distribution resulted from the small Fermi energy in the emitter, determined mostly by

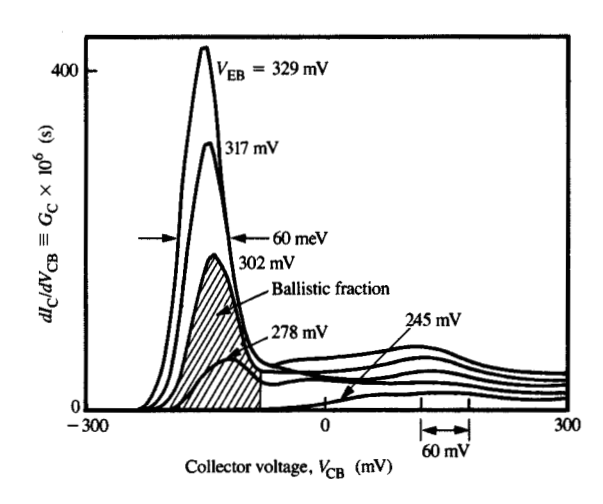
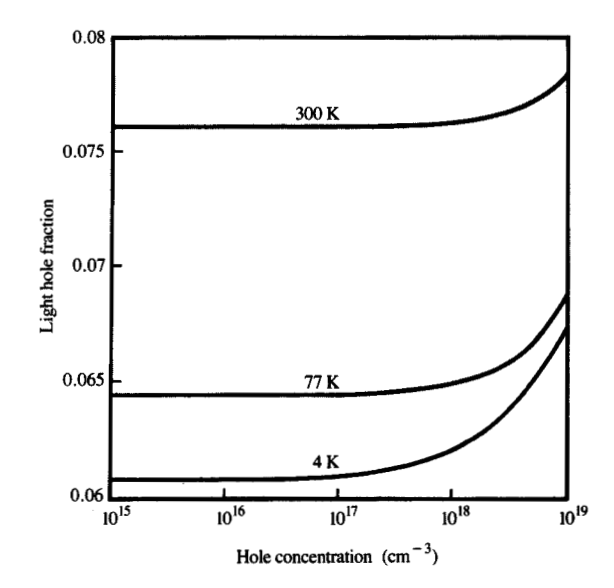
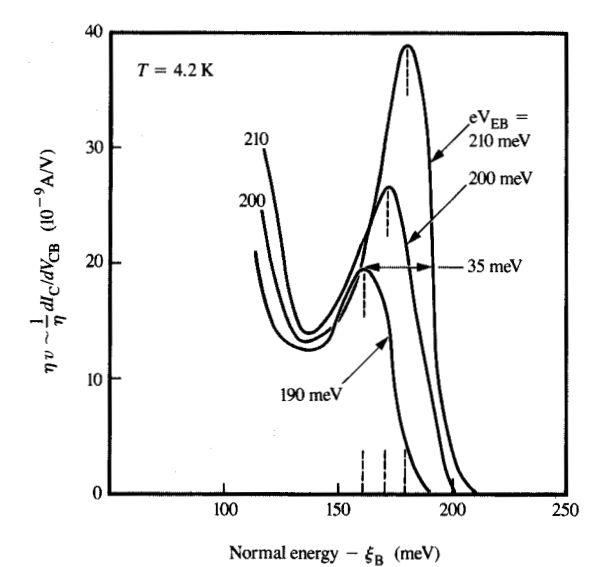


Figure 5

Derivative of collector current vs. collector voltage, with injection voltage as a parameter, for the THETA device of Figure 7. Although the distributions shown are the momentum distributions $n\nu(E)$ of the ballistic electrons, they are similar to the energy distributions n(E) if the electron velocity at the injector is almost constant over the 60-meV width. From [8], reproduced with permission.



Fraction of light holes relative to the total hole population in a p-type $(2\times10^{18}\,{\rm cm}^{-3})$ THETA device, at three temperatures.



Energy distributions of ballistic light holes after traversing 31 nm of a heavily p-doped GaAs base region, and about 20 nm of an undoped AlGaAs collector barrier. Note the lower-energy tails of the distributions, indicating the presence of hot, nonballistic holes. From [10], reproduced with permission.

the presence of the heavy holes. As is shown in a later section, the ballistic holes were found to be light.

Coherent effects in the THETA device

If the length of the transport region is of the same order of magnitude as the wavelength of the traversing electrons, only a relatively small number of normal electron momentum states p_{\perp} are allowed in the region. Consequently, the electronic charge and potential distribution in the region are expected to deviate from the classical case. Also, the energy dependence of the probability for electron tunneling into these regions should contain strong resonances as a function of injection energy (assuming the transverse momentum is preserved in the tunneling process). These sizequantization effects should affect the transport if the energy separations between the bottoms of sequential sub-bands are comparable to the energy width of the normal injected distributions. We also expect that the usual bulk scattering events should be strongly modified because of these size-quantization effects, but we do not discuss that here.

Formulation

In wide regions of the device, the potential distribution can be obtained by solving the Poisson equation, and treating the electrons classically in the Thomas-Fermi approximation. However, for some regions of the device, this is not suitable. Figure 11 illustrates this situation: Considering one of our structures with a base width of 29 nm, we have solved the Poisson equation using the classical electron charge density shown in the lower portion of Figure 11(a) and have obtained the potential distribution shown in the upper portion. We have also solved the Poisson equation employing the charge density corresponding to the quantized electrons in the base, as illustrated in Figure 11(b). The Poisson and Schrödinger equations must be solved self-consistently because the electron wave functions $\zeta(x)$ (ν being the index of the sub-band of energy E) depend on the potential distribution V(x), which, in turn, depends on the charge density $e|\zeta_{\parallel}|^2$.

The form of the Poisson equation to be solved is

$$\frac{d}{dx} \left[\varepsilon(x) \frac{dV(x)}{dx} \right]$$

$$= e \left\{ \hat{F}_{1/2} [(E_{\rm F} - E_{\rm C} - eV(x))/(k_{\rm B}T)] - N_{\rm D} \right\}, \tag{7a}$$

$$\frac{d}{dx} \left[e(x) \frac{dV(x)}{dx} \right] \tag{7b}$$

$$=e\left\{N_{2}\sum_{\nu}\hat{F}_{\nu}[(E_{\mathrm{F}}-E_{\mathrm{C}})/(k_{\mathrm{B}}T)]\left|\left.\zeta_{\nu}(x)\right.\right|^{2}-N_{\mathrm{D}}\right\},$$

where Equation (7a) is valid in regions where electron quantization effects are neglected and Equation (7b) is valid for the (quantized) free electrons in the base region. In the equations above, $N_{\rm D}$ is the concentration of ionized donors, $\varepsilon(x)$ is the dielectric constant, $E_{\rm C}$ is the bottom of the Γ band, and the equivalent density-of-states factors $N_{\rm C}$ and $N_{\rm C}$ are given by

$$N_C = 2[(2\pi m_{C0} k_{\rm B} T)/(2\pi \hbar)^2]^{2/3}$$
 (8)

for the electrons in the bulk, three-dimensional emitter and collector, and

$$N_2 = \frac{m_{C,0} k_{\rm B} T}{\pi \hbar^2} \tag{9}$$

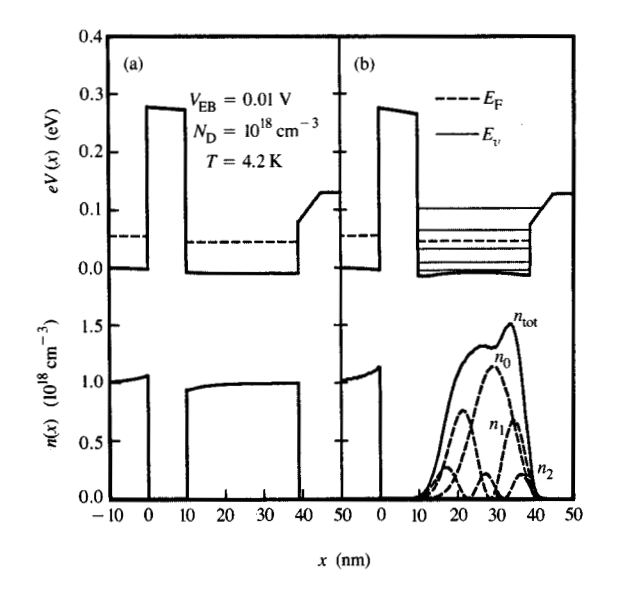
for the two-dimensional electron gas in the base.

The two-dimensional Fermi integral is

$$\hat{F}_{\nu}(\eta_{\rm F}) = \int_0^\infty d\eta \, \frac{\theta[\eta - E_{\nu}/(k_{\rm B}T)](1 - 2\eta\beta)}{\exp(\eta - \eta_{\rm F}) + 1}.$$
 (10)

The nonparabolicity of the central valley has been accounted for by $\beta = \gamma k_{\rm B} T$, where γ is the usual nonparabolicity coefficient. The function $\theta(x)$ is the usual step function.

The Schrödinger equation, accounting for nonparabolicity effects via an energy-dependent effective mass $m_{\rm en}$, takes the form





Classical (a) and self-consistent (b) solutions of the Poisson equation for a THETA device. Note the different shape of the self-consistent potential in the base region and the shift of the Fermi energy at the AlGaAs-base interfaces. Also shown are the associated charge distributions; the presence of three occupied sub-bands is indicated for the self-consistent solution.

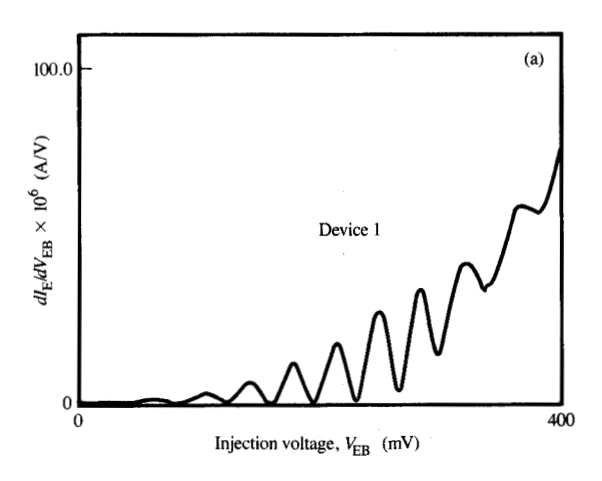
$$\frac{d}{dx}\left\{\frac{1}{m_{\rm en}[E-eV(x)]}\frac{d\zeta(x)}{dx}\right\} = \frac{2}{\hbar^2}\left[E-eV(x)\right]\zeta(x),\tag{11}$$

with the normalization condition $\int dx |\zeta(x)|^2 = 1$. For both Equations (7) and (11), we have imposed continuity of the electric displacement fields and electron phase velocities at the heterojunctions. The nonparabolic corrections in Equation (11) are treated approximately and yield a rigorously correct result in the case of plane waves, as is approximately applicable to the base of a THETA device.

Results

The coupled equations (7) and (11) can be solved numerically by an almost standard iteration procedure. Typically, 8 to 12 iterations are necessary to obtain convergence.

Experimentally, the bound states in the base region of the THETA were observed experimentally by the appearance of resonances in the emitter or base currents, and a modulation in the transfer ratio of the device. Figures 12(a) and 12(b) show typical experimental results. The numerical derivative of the emitter current with respect to the injection voltage $V_{\rm FB}$ is plotted in



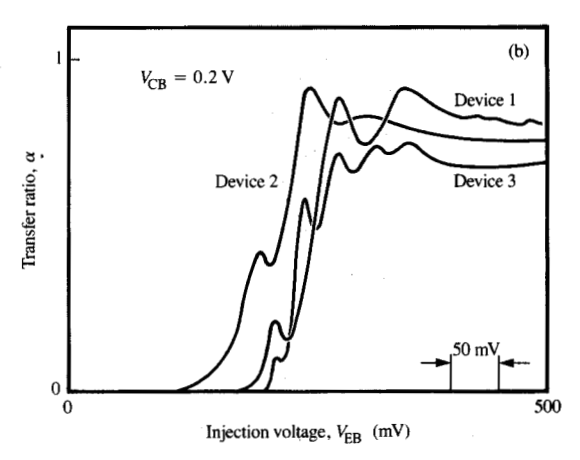
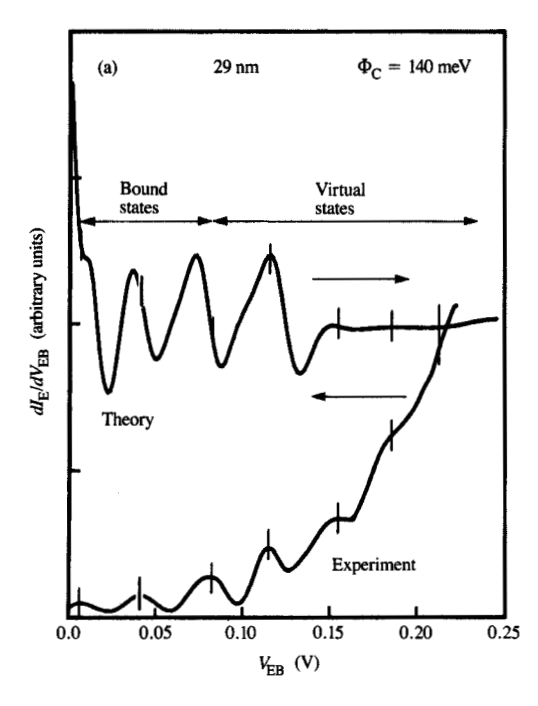
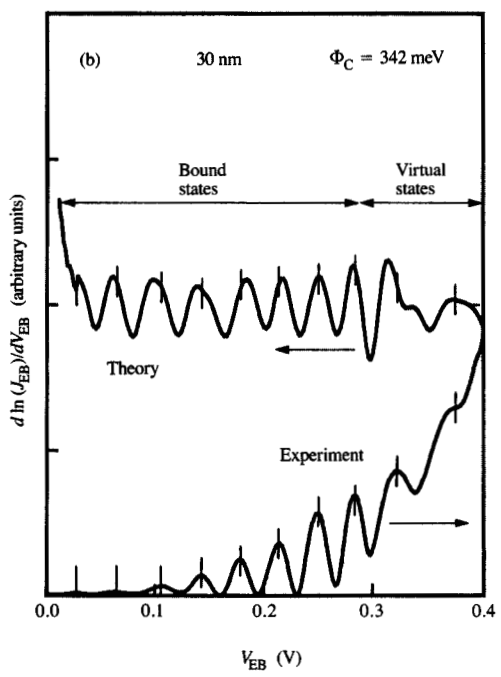


Figure 12

(a) Derivative of emitter current $I_{\rm E}$ with respect to the injection voltage $V_{\rm EB}$ of a THETA device having a 30-nm-wide GaAs base region, doped to a concentration of 1×10^{18} cm $^{-3}$, and a confining collector with a barrier height of about 260 meV. The oscillations correspond to bound states ($V_{\rm EB} < 220$ mV) and to virtual states ($V_{\rm EB} > 220$ mV) in the base region. (b) Transfer ratios of that device and two others, indicating that the virtual states are also "sensed" by those ratios. The onset of transfer indicates the collector barrier height above the Fermi level in the base at $V_{\rm CB} = 0.2$ V.

Figure 12(a), showing clear peaks associated with quantum levels in the base. In addition, structure associated with quantum reflections at the interfaces is present, arising from electrons injected at energies above the confining barrier between the base and collector. The structure is associated with what we refer to as "resonant," "virtual," or "unbound" states. Figure 12(b) shows the effect of the virtual states on the transfer ratios of three devices. The observation of these states is very interesting because their existence necessitates that phase





Experimental $dI_{\rm E}/dV_{\rm EB}$ curves and theoretical logarithmic derivatives of the tunneling current for two narrow-base THETA devices [in (a) and (b)]. Both the bound and unbound states regions are illustrated. A self-consistent Poisson–Schrödinger solution for the potential and Equation (3) was used in a numerical simulation; a fit to relatively high band energies can be seen in (b). From [22], reproduced with permission.

coherence be maintained by the electrons as they cross the device; i.e., ballistic transport must be occurring.

For the numerical calculations, we integrated the tunneling probability over the Fermi distribution of the electrons in the emitter for each bias point. Then a numerical derivative with respect to the bias was obtained. As can be seen in **Figure 13**, the numerical resonances appeared at the expected biases up to relatively high energies. From that a value could be obtained for the nonparabolicity parameter, γ . Only when use was made of a value of -0.834, which is very close to that obtained from empirical pseudopotential calculations, was there good agreement between the numerical calculations and the experimental results, as can be seen for the two devices characterized in parts (a) and (b) of the figure.

This is a unique and powerful way to determine the effective mass up to relatively high electron energies. At such energies, many of the electrons occupy the upper satellite valleys (the L and X valleys), and the effective masses associated with the satellite valleys are difficult to isolate. Since the resonances resulted only from the ballistic, coherent, " Γ electrons," we were thus able to measure the effective mass associated with the Γ valley.

• Interference of ballistic holes

Similar quantum interference resonances have also been observed in p-type THETA devices, resulting from ballistic holes traversing the base [10]. The resonances observed at several collector voltages can be seen in Figure 14. The number of resonances in the bound regime and their energies agreed well with simple calculations assuming transport by light holes of constant mass in a one-dimensional rectangular box. This unequivocally confirms that the ballistic holes are light. If the holes were heavy, at least sixteen sub-bands would have been observed. The observed bound states are distinguished from the virtual ones by the strength of the resonances. It can be seen in the figure that as the collector voltage becomes negative, the associated potential barrier and the number of bound states both decrease. As has been indicated previously for ballistic electrons in the n-type devices, the presence of strong resonances constitutes another indication for the existence of ballistic holes in the p-type devices.

Scattering of hot electrons

On the basis of their experimental results, Hollis et al. [15(b)] have suggested that the dominant scattering of hot electrons occurs through interaction with coupled modes of plasmons and optical phonons. This hypothesis was later on adopted by Levi et al. [7, 25], who calculated an MFP of about 30 nm for hot electrons with excess kinetic

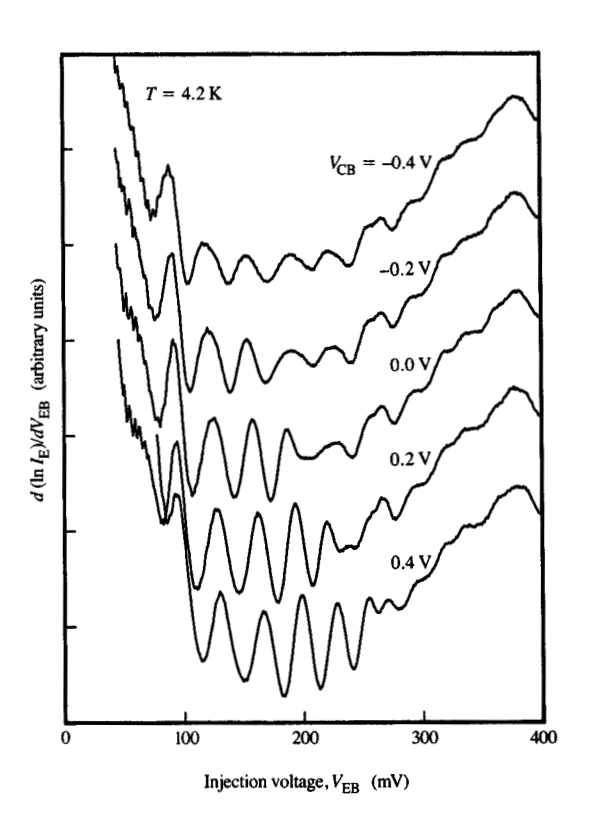
energy of 250 meV in layers doped to a level of 1×10^{18} cm⁻³. But the calculations were carried out for hot electrons traversing bulk GaAs, while in reality the transport occurred through very thin layers. The calculation of the scattering rates in thin layers, however, is nontrivial, since there are only a few sub-bands in a narrow base; this number is neither too large to justify a bulk, three-dimensional approximation [7, 25], nor small enough to simplify the calculation of relevant quantities. In any case, we should expect that as the base-width decreases, the MFP should increase: The smaller twodimensional density of the final states for the elementary excitations, and the weaker matrix elements between the incident hot-electron state (with momentum mainly in the direction normal to the interfaces) and the excitations in the base (mostly with momentum parallel to the interfaces), should reduce the scattering rates.

Also difficult is an experimental determination of the MFP in a uniformly doped, thin, confined layer. In addition to fundamental scattering events, the net transfer of ballistic electrons is affected by quantum-mechanical reflections from the base-collector barrier interface, alloy scattering in the AlGaAs collector barrier, and some transfer of electrons into the L valleys. Another effect that complicates matters is a lack of knowledge of the participating length of the doped base during electron injection. As the injection voltage across the tunneling barrier increases, a substantial part of the base becomes depleted, making the transport region highly nonuniform.

♦ Electron-electron scattering

It was noticed early in the work on the THETA device that its gain is inversely proportional to the doping level in its base. From studies on a number of devices produced over a period of time, it appears that as the doping level is decreased from 2 to 0.2×10^{18} cm⁻³, the current gain rises and saturates. For devices in which the base width was about 30 nm, the current gain [$\beta = (dI_C/dI_B)$] approached 15 when the injection energy reached the Γ -L energy separation. It is clear that higher gains could be achieved if the L valleys were higher in energy, since scattering cross sections decrease with increasing injection energy. As discussed previously, hotelectron-cold-electron or hot-electron-plasmon scattering events were probably dominant in these devices.

Devices with such narrow bases and lower base doping levels are very difficult to fabricate, since the base resistance becomes very high. Replacing the GaAs base with a pseudomorphic InGaAs base (described later) increases the Γ -L energy separation and leads to an increased gain at higher injection energies, even at a base doping level of about 10^{18} cm⁻³.

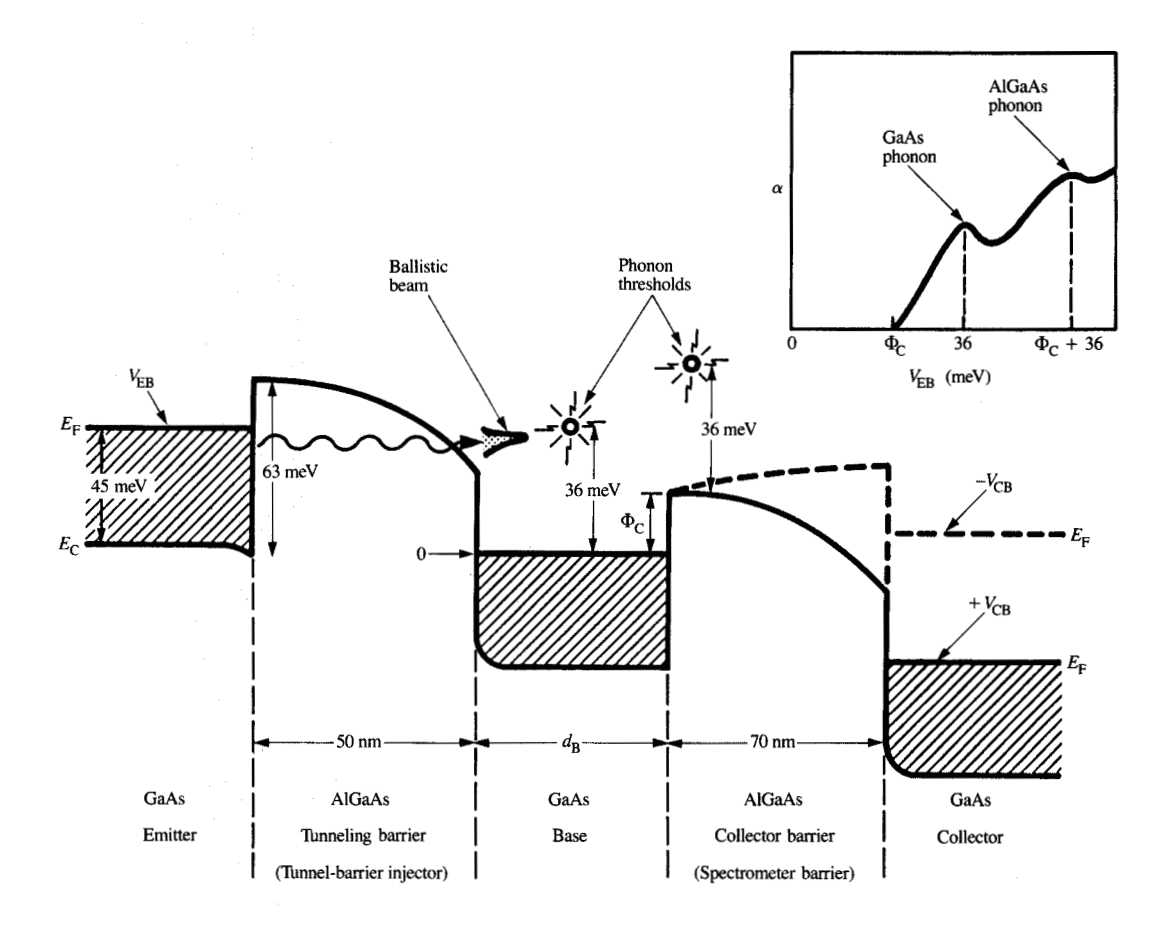


Bieune de

Resonances in the tunneling currents into the confined base of a p-type THETA device. The peaks exhibit bound (strong) and virtual (weaker) states, which change as the collector barrier is biased and the confining well changes. The spacings indicate transport predominantly by light poles. From [10], reproduced with permission.

• Optical phonon emission

Among the variety of phonons in GaAs, the longitudinal optical (LO) phonons are coupled most strongly to lowenergy electrons. The nature of the scattering process is such that electrons tend to maintain their original direction. Strikingly, in all of our spectroscopy work, phonon replicas were never detected. To detect phonon emission, THETA structures with very low spectrometer barrier heights (less than the phonon energy), were fabricated (Figure 15). Tunnel-barrier injectors, 50 nm thick, with a 7% AlAs mole fraction in the AlGaAs alloy, produced an injected energy distribution about 4 meV wide [26]. The spectrometer barrier in that case was 70 nm thick, with a similar AlAs mole fraction and a barrier height of about 73 meV (due to some unintentional negative charges in the AlGaAs); the barrier height was about 28 meV above the Fermi level in the base.



Use of a THETA device having relatively thick barriers and a low AlAs mole fraction (7%) in order to detect LO phonon emission. From [26], reproduced with permission.

Single LO phonon emission was detected when the injection energy above the Fermi level in the base exceeded 36 meV (the small wave-vector LO phonon energy). The behavior of the transfer ratio α observed for structures with base widths of 52 nm and 32 nm is seen in Figure 16. Note that α rises rapidly when the injection energy $eV_{\rm FR}$ exceeds the spectrometer barrier height $\Phi_{\rm C}$. When $eV_{EB} = 36$ meV, α drops sharply, reaching a minimum around 40 meV, and then increases. The drop in α beyond $V_{\rm EB} = 36$ mV is due to the ballistic electrons which emit a phonon, lose 36 meV of energy, and remain uncollected. The overall monotonic rise of α is determined by the energy dependence of all of the scattering mechanisms which are active. In particular, the quantum-mechanical reflections from the basespectrometer interface are dominant for energies close to the spectrometer barrier height.

We define the fractional loss of electrons at energy E(determined by $V_{\rm EB}$) due to phonon emission as $\alpha_{\min}(E)/\alpha_{\max}(E)$, where $\alpha_{\min}(E)$ and $\alpha_{\max}(E)$ are measured and extrapolated values, as for example in Figure 16. [The $\alpha_{max}(E)$ are values of $\alpha(E)$ in the absence of phonon emission.] The different slopes of $\alpha(E)$ before and after threshold indicate an increase in the scattering rate as the electron energy increases. To minimize the error in our estimate for the scattering rates deduced from the extrapolated $\alpha_{max}(E)$, we measure $\alpha_{min}/\alpha_{max}$ at the lowest possible energy above threshold, namely, about one distribution width above the threshold energy. We estimate the MFP (designated here as λ) from Figure 16 by using $\exp(-d_B/\lambda) = \alpha_{\min}(E)/\alpha_{\max}(E)$, where d_B is the base width. At an energy of about 85 meV we find that $\lambda \simeq 126$ nm and $\lambda \simeq 130$ nm for structures with base widths of 52 nm and 32 nm, respectively. Since at 85

meV the ballistic electron velocity is about 6.1×10^7 cm/s, we deduce a scattering time τ of about 210 fs for phonon emission at that energy in the n⁺ GaAs layers. At slightly higher energies, for example 90 meV, we find that $\lambda \simeq 115$ nm and $\tau \simeq 185$ fs.

These results agree with calculated and measured scattering rates in undoped GaAs. The agreement is somewhat surprising, since at the equilibrium electron concentration in a base having a doping level of 8×10^{17} cm⁻³, the LO phonons and plasmons have similar energies ($\hbar\omega_{\rm plas} \simeq 38$ meV, where $\omega_{\rm plas}$ is the plasma frequency), and thus interact strongly, resulting in the appearance of two coupled modes (a plasmon-like mode with $\hbar\omega = 43$ meV and a phonon-like mode with $\hbar\omega =$ 28 meV at q = 0 [27]). The lowest possible value of q for modes participating in the scattering is $\approx 1 \times 10^6$ cm⁻¹, leading to two possibly observable thresholds: a plasmonlike threshold at \approx 57 meV and a phonon-like one at \approx 30 meV. Experimentally, neither was observed. Screening and the emission of higher-wave-vector LO phonons (with $\hbar\omega_{LO} \simeq 36$ meV) might explain the observed 36-meV peak and the scattering cross sections that

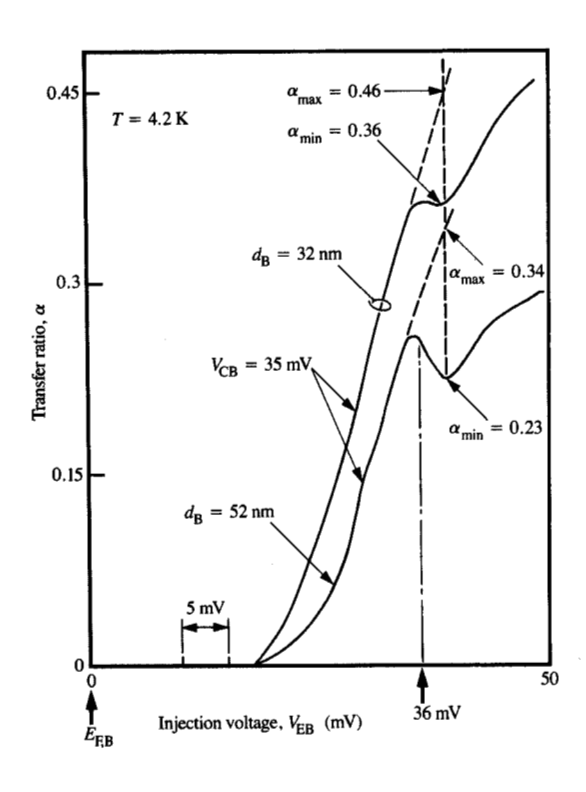
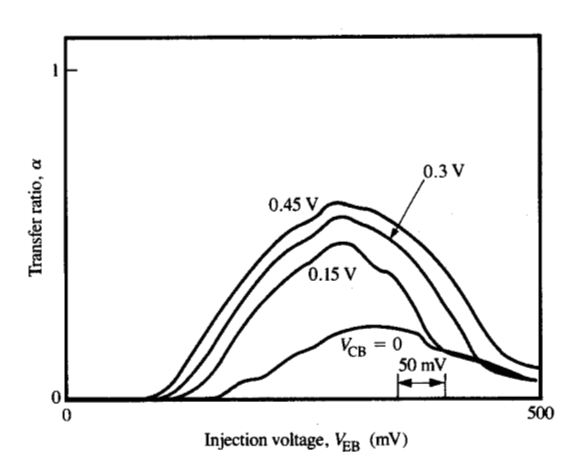


Figure 16

Transfer ratio of two THETA devices having base widths of 32 nm and 52 nm, respectively. Thresholds due to phonon emission are clearly seen. From [26], reproduced with permission.



DOMEST OF

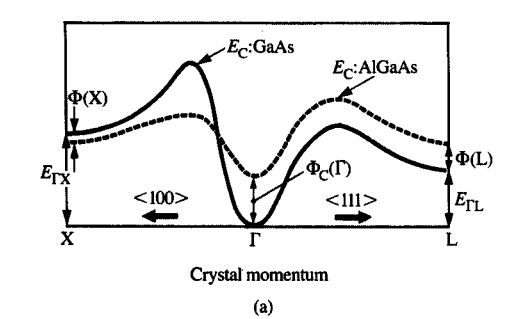
Transfer ratio of a THETA device having an 80-nm-wide base and an abrupt collector barrier. Note how the transfer ratio drops drastically when the injection energy exceeds a value somewhat below 300 mV, independently of the collector biasing voltage.

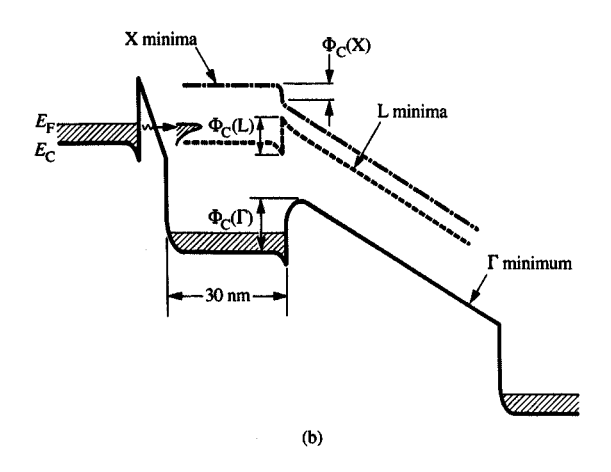
fortuitously agree with those for undoped material [28]. However, the reason for the absence of a threshold at 57 meV is not clear. Similarly, single optical phonon emission has been observed in undoped AlGaAs using THETA devices [26].

• Transfer to the L valleys

Figure 17 shows the differential transfer ratio α as a function of injection voltage $V_{\rm EB}$, measured with a THETA device having a 30% AlAs mole fraction in its collector barrier and a base width of 80 nm. As can be seen, α decreases sharply above some injection voltage threshold $V_{\rm tr}$. We attribute this effect to the transfer, as a result of scattering, of otherwise ballistic electrons into the six L valleys in GaAs, having minima at the edge of the Brillouin zone in the $\langle 111 \rangle$ direction. The separation in energy between the Γ valley and the L valleys is about 0.3 eV. Electrons that transfer from the former to the latter require an added crystal momentum of π/a in the $\langle 111 \rangle$ direction, where a is the lattice constant in the $\langle 111 \rangle$ direction.

At low temperatures, this added momentum can most likely be gained by the emission of zone-edge phonons. Electrons that transfer into the L valleys and remain there while traversing the base encounter a potential barrier at the base-collector barrier interface and are not collected (see **Figure 18**). Assuming the presence of zone-edge phonons of 28 meV, a deformation potential





(a) Comparative conduction-band edges in GaAs and AlGaAs versus crystal momentum. (b) Relevant band edges, etc., in a THETA device. The electrons in the L valleys experience a barrier $\Phi_{\rm C}({\rm L})$ which must be surmounted before collection is possible. The electrons in the X valleys experience a ''negative'' barrier $\Phi_{\rm C}({\rm X})$ at the same interface. From [29], reproduced with permission.

coupling coefficient $D_{\Gamma L} = 7 \times 10^8$ eV/cm, and the availability of excess energy above the threshold for transfer of 0.1 eV of energy, we find a scattering time $\tau(\Gamma \to L) \simeq 120$ fs. Conversely, for the reverse, we find $\tau(L \to \Gamma) \simeq 1$ ps. If the velocity of the ballistic electrons is assumed to be 1×10^8 cm/s, about 10% of the ballistic electrons having kinetic energy of about 0.4 eV would be expected to transfer to the L valleys in a 10-nm traversal distance [29].

From the observed transfer ratio, the valley separation $E_{\Gamma L}$ can be determined to be \approx 0.29 eV, in close agreement with known data. Similar results have been obtained by Hase et al. [30]. Note that transfer into the X valleys (at injection energies above 510 meV) was not observed. This is most probably due to the absence of a potential barrier for the "X electrons" at the collector

barrier interface [since $\Phi_{C}(X) < 0$, as can be seen in Figure 18].

To verify that the behavior described above is indeed due to intervalley transfer, we have applied hydrostatic pressure to several devices which were cooled to 77 K. The locations in energy of the Γ , L, and X valleys increase differently with pressure, leading to a change in their energy separation $\Delta E_{\rm PL}$ of about -5.5 meV/kbar [31]. Figure 19 shows the observed change in α versus $V_{\rm EB}$ of a device with a base width of 30 nm when the pressure P was increased to 10.8 kbar at a fixed collector voltage. It can be seen that $V_{\rm th}$ decreased as the pressure was increased. At the maximum pressure, the onset for transfer decreased by about 60 mV, as expected. Moreover, the fraction of electrons that transferred increased with pressure. Note that the onset of α in V_{FR} is invariant, indicating that the barrier height $\Phi_{c}(\Gamma)$, and thus also the band discontinuity, are unaffected by hydrostatic pressure.

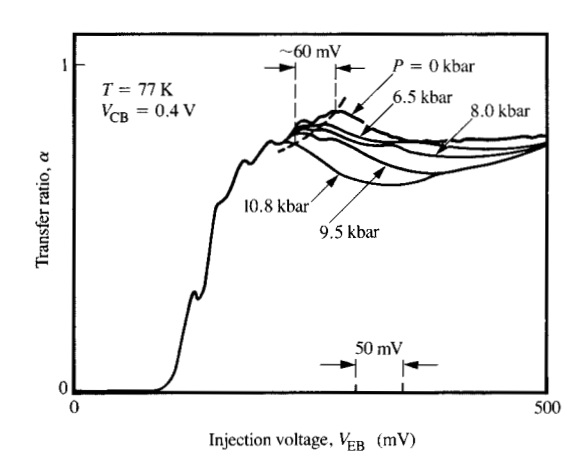
Alloy scattering

Since the collector is biased positively with respect to the base when the device is operated as an amplifier, scattering in the collector barrier is not apparent, because the scattered electrons relax to the bottom of the conduction band in the barrier and "roll down" to the collector contact. Thus, it is difficult to distinguish between the scattered electrons and the ballistic ones. However, when a negative voltage is applied to the collector, the scattered electrons "roll back" to the base and the collector current drops more rapidly. This behavior is seen in Figure 20, in which the derivative of the collector current is plotted with respect to the collector voltage, revealing a peak near $V_{\rm CB} = 0$. It is interesting to note that the ballistic peak (toward the left) shifts appropriately as the injection energy increases, but decreases in magnitude relative to the "alloy scattering peak," which increases in magnitude but does not shift in energy. An increase in the alloy scattering cross section is expected from a density-of-states consideration (which increases as $E^{1/2}$) [32].

The THETA device as an amplifier

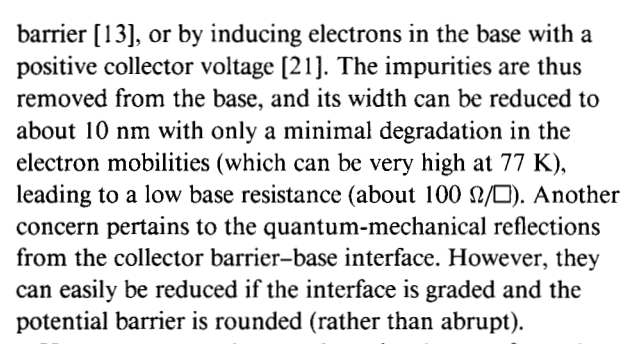
A concern regarding hot-electron devices had for some time been their relatively low gain. The reason for this is their sensitivity to the normal energy associated with the hot electrons. Thus, even a direction change resulting from elastic scattering events tends to reduce their gain.

As mentioned previously, reducing the doping level in the base of a THETA device leads to an increase in its gain. However, this leads to an increase in base resistance and creates an unwanted coupling between input and output. This can be partially overcome by selectively doping the base, by introducing donors in the collector



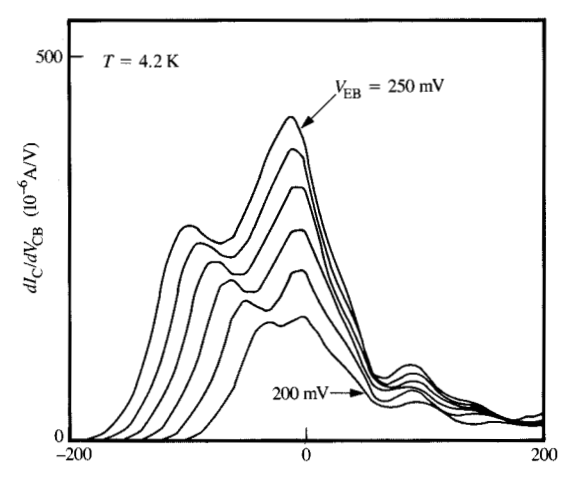


Dependence of transfer ratio on injection voltage at different hydrostatic pressures, measured at 77 K. The onset for transfer and the resonances do not change, but $V_{\rm th}$ decreases by about 60 mV as the pressure is increased from 0 to 10.8 kbar. From [29], reproduced with permission.



However, as was also noted previously, transfer to the L valleys is the biggest obstacle to increasing the gain. We next describe an InGaAs pseudomorphic base device that partly overcomes this difficulty.

• A pseudomorphic InGaAs-base THETA device Although the lattice constant of InGaAs is greater than that of GaAs, thin layers of InGaAs can be grown pseudomorphically on GaAs. For an InAs mole fraction of about 15%, layers as thick as 20 nm can be grown without dislocations. The advantage in using these layers for the base of a THETA device is twofold: the Γ -L energy separation is greater, and a lower AlAs mole fraction in the collector barrier can be used, thus improving the quality of the barrier. This is possible due to an added conduction-band discontinuity between the InGaAs and the GaAs.



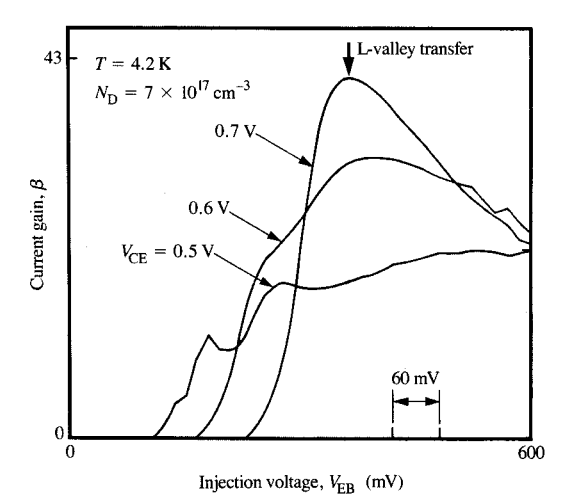
Spectrometer voltage, V_{CB} (mV)

Figure 20

Derivative of collector current with respect to spectrometer voltage. Two peaks are seen—a ballistic peak that shifts to higher energies as the injection energy increases and one near $V_{\rm CB}=0$ which grows in amplitude relative to the ballistic peak. The latter phenomenon is due to alloy scattering.

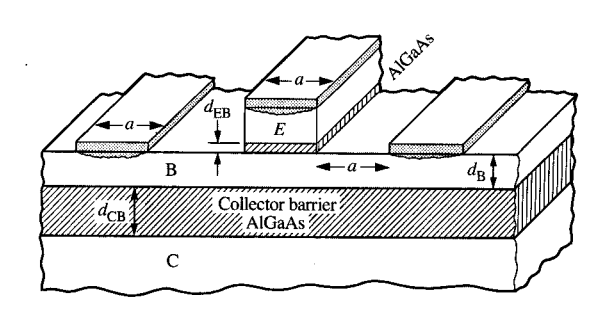
THETA devices with an InGaAs base having an InAs mole fraction of 12–15% and base thickness of 20–30 nm have been fabricated and have shown considerably higher gains than GaAs devices with a similar base doping level (10^{18} cm⁻³). We have found resulting Γ –L energy separations of 380 meV and 410 meV for InAs mole fractions of 12% and 15%, respectively. We have also found a conduction-band discontinuity between GaAs and $\ln_x Ga_{1-x}$ As of ΔE_C (meV) = 7.5x (%) [33, 34]. In devices with a base width of 21 nm and a doping level of 8×10^{17} cm⁻³, an InAs mole fraction of 12% in the base, and an AlAs mole fraction of 10% in the collector, current gains as high as 30 and 41 were measured at 77 K and 4.2 K, respectively.

The current gain for a pseudomorphic THETA device versus injection voltage at 4.2 K is shown in Figure 21. This gain is the highest reported thus far for a vertically configured hot-electron device. Since the main difference between the devices and those discussed previously was in their Γ -L energy separations (corresponding effective masses and scattering cross sections are expected to be similar), the dramatic increase in gain that was achieved was most likely due to that difference. It can be seen in Figure 21 that the gain drops sharply when the injection energy increases above a level corresponding to the



Biginia 2

Current gain at 4.2 K of an InGaAs pseudomorphic-base THETA device (InAs mole fraction of 12%) vs. injection voltage, operating in a common-emitter configuration, at different collector voltages. The maximum gain of about 40 occurs at the threshold of transfer into the L valleys. From [34], reproduced with permission.



Schematic of a THETA device, depicting electrode width and spacing a, barrier thickness $d_{\rm EB}$, base width $d_{\rm B}$, and collector width $d_{\rm CR}$.

bottom of the L valleys. Note, however, that the output characteristics of such devices operating in a common emitter configuration exhibit a relatively high output conductance.

• Potential speed

The transit time of the intrinsic THETA device is composed of three components: the time required for carrier transit through the tunnel-barrier injector (less than 10 fs [35]), the time $\tau_{\rm B}$ required for carrier transit through the base (30 fs through a 30-nm-wide base), and the time $\tau_{\rm C}$ required for carrier transit through the collector barrier (250 fs through a 50-nm-wide collector barrier, assuming a group velocity of 2×10^7 cm/s). The total transit time, which is less than 0.3 ps, is usually smaller than the time constants imposed by the parasitic capacitances and the dynamic charges that must be transferred in and out of the base of an actual device in every switching cycle.

The latter can be calculated by examining the change of the stored charge in the base,

$$\Delta Q_{\rm R} = C_{\rm FR} \Delta V_{\rm FR} + C_{\rm CR} \Delta V_{\rm CR} + i_{\rm C} \tau_{\rm R} + i_{\rm C} \tau_{\rm C} + i_{\rm R} \tau_{\rm R}'. \tag{12}$$

The first and second terms represent the charges at the emitter and collector barriers; the third term represents the dynamic charge in the base; the fourth term represents the dynamic charge in the collector barrier; and the last term represents the charge that thermalizes in the base (since it is a function of position, a modified transit time τ_B' rather than τ_B must be used). This charge must be supplied by the base current i_B ; thus $\Delta Q_B = i_B \Delta t$. If $\Delta V_{CB} = 2\Delta V_{EB} = \Delta V$ and the dynamic charges are neglected, for a current source supplying charge to the base, the switching time is expected to be

$$\Delta t \simeq \frac{\Delta V}{i_{\rm B}} (C_{\rm EB} + 2C_{\rm CB}). \tag{13}$$

However, if the base is fed by a voltage source, and we assume a base resistance $R_{\rm B}$ such that $i_{\rm B}R_{\rm B}=\Delta V$, we obtain a switching time

$$\Delta t \simeq C_{\rm FR} R_{\rm R} + 2C_{\rm CR} R_{\rm R} \,. \tag{14}$$

Referring to **Figure 22**, in an "aggressive" device, $a=0.25~\mu\text{m}$, $d_{\text{EB}}=10~\text{nm}$, $d_{\text{B}}=30~\text{nm}$, and $d_{\text{CB}}=50~\text{nm}$. For such a device, we calculate $\Delta t=1~\text{ps}$ for a voltage swing ΔV of 0.1 V, and a base current density of $2\times10^5~\text{A/cm}^2$. For a voltage source for a base having a resistivity of $500~\Omega/\square$, we calculate a switching time of 0.6 ps. In both modes of operation, the times should be less for a self-aligned configuration. If the base is selectively doped and the mobility at 77 K is $40\times10^3~\text{cm}^2/\text{V-s}$, a sheet resistivity of about $100~\Omega/\square$ should be achievable, leading to a much shorter $R_{\text{B}}C$ time constant.

The p-type THETA device should be almost as fast as the n-type device because of the light nature of the ballistic holes. Its main drawback is its high base resistance, governed by the dominance of heavy holes, but this can be circumvented by selectively doping the base, thus increasing the mobility of the heavy holes.

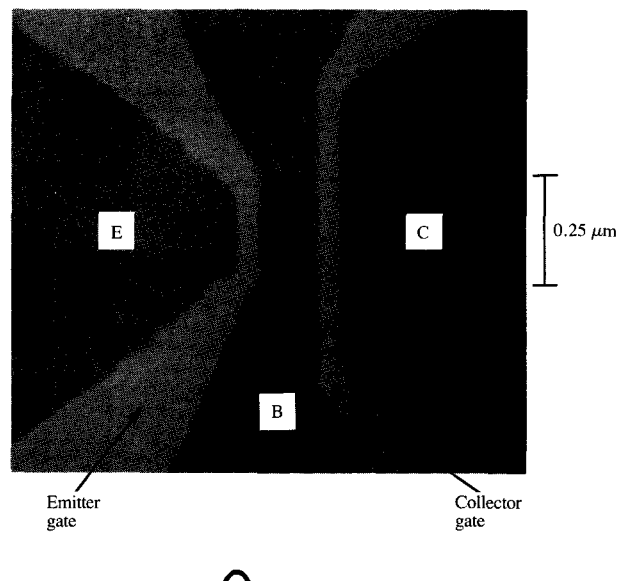
A lateral THETA device

There are appreciable difficulties in properly fabricating a vertically configured hot-electron device (e.g., the etching of its layers with precise termination and achieving accurate penetration of its ohmic contacts)—thereby achieving a long mean free path and, hence, a high gain. Fabricating planar versions of such devices alleviates some of the difficulties.

In that regard, a laterally configured version of the THETA device has recently been fabricated [36] which is based on transit in the plane of a two-dimensional electron gas (2DEG). The high mobility of electrons in a 2DEG, as a result of the remoteness of impurities, is conducive to achieving a long MFP—thus potentially leading to a high device gain. Barriers were fabricated by inducing potential barriers using very short metal gates deposited on the surface of a heterojunction structure containing a 2DEG. As in the case of an MOS device, applying a negative voltage to a gate with respect to the 2DEG depletes the carriers beneath and raises the bottom of the conduction band with respect to the Fermi level. When the bias on the gate exceeds a certain value, depletion is complete, and a barrier is created for the electrons which reside on both sides of the gate. Formation of two narrow gates on the surface, each biased negatively with respect to the 2DEG, creates a structure which has a potential profile similar to that of the vertical THETA device. One potential barrier, approximately parabolic in shape, is employed as the tunnel-barrier injector, while the other is used as the collector barrier.

The device, with its gates and emitter, base, and collector regions, is depicted in Figure 23. Since the potential barriers are about 50 nm thick (determined by the length of the nano-gates and their distance from the 2DEG), their heights must be low (about 50 meV) to obtain suitable tunneling current densities. Thus the injected distributions are expected to be rather narrow—less than 5 meV in width. Similar two-terminal structures have recently been fabricated to search for resonant tunneling in the plane of a 2DEG, leading to an indication of some spatial quantization [37, 38].

Also shown in Figure 23 is the corresponding potential distribution in the 2DEG. The emitter is made narrower than the collector in order to maximize α , namely, to permit collection of most of the electrons that emerge laterally from the emitter barrier. In **Figure 24** are shown the output characteristics of the lateral THETA device of Figure 23. The transfer ratio of the device at 4.2 K was found to be about 0.9 [36, 39] with a collected ballistic fraction, deduced from spectroscopy measurements, of about 0.7, leading to an MFP of about 0.5 μ m for injection energies below the LO phonon energy. Ballistic distributions having a full width half maximum (FWHM) of about 4 meV were obtained.



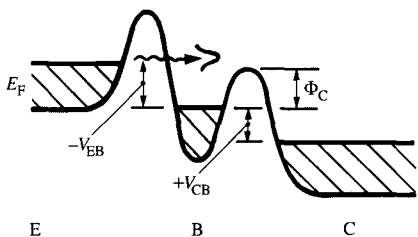


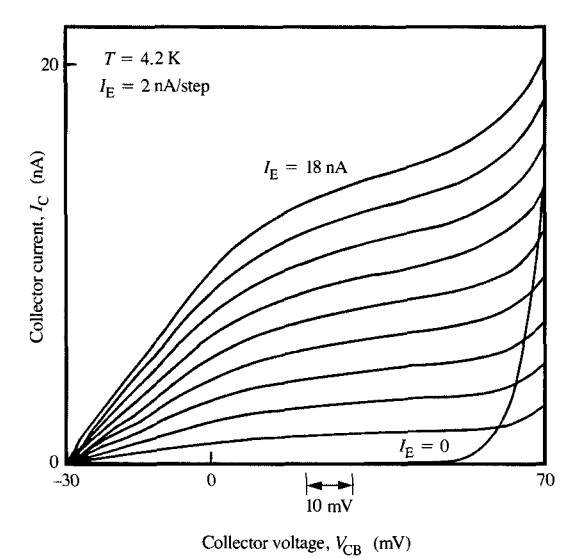
Figure 28

An SEM micrograph of a lateral THETA device. The width of the emitter gate is $0.25~\mu m$, and that of the collector gate is $0.75~\mu m$; the base length is $0.17~\mu m$. Below is shown a schematic of a potential distribution, assuming a negatively biased emitter, a positively biased collector (with respect to the base), and negatively biased gates. From [39], reproduced with permission.

By adding two gates adjacent to the emitter gate and applying a negative voltage to those gates, tunneling could be limited to the forward direction (Figure 25), resulting in a higher maximum gain. It was thereby possible to increase the current gain of the device to about 100, thus realizing the high-gain potential anticipated because of the use of the two-dimensional electron gas configuration.

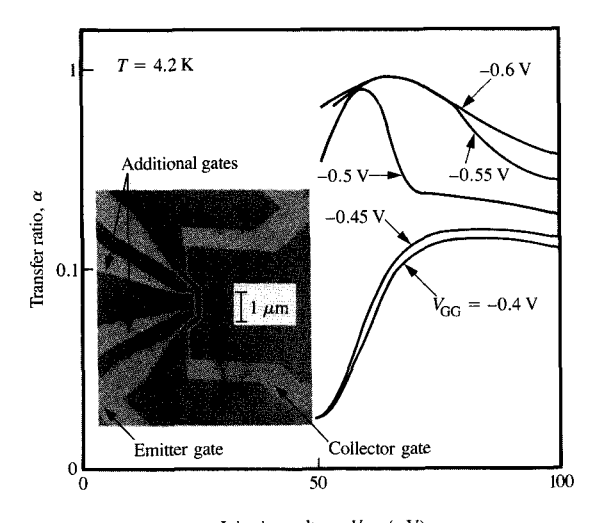
Concluding comments

As the lateral dimensions of semiconductor devices approach the submicron range, their electrons will become hotter, and will traverse the devices more ballistically and quasi-ballistically. Although clear experimental data and a reliable theoretical treatment of high-energy electron transport properties are not yet in hand, the use of hot-electron devices utilizing ballistic



Firming 24

Output I-V characteristics of the device of Figure 23, operating in a common base configuration. The maximum current gain is about 0.9, and the ballistic fraction is about 0.75. From [39], reproduced with permission.



Injection voltage, V_{EB} (mV)

Emme

Effect on the transfer ratio of the addition of the gates shown in the insert. The additional gates were biased at $V_{\rm GG}$ with respect to the base. The maximum current gain could thus be increased to about 100. From [39], reproduced with permission.

transport is providing a powerful means to fill this gap. We have seen how electronic phenomena (such as the nonparabolicity of bands) and transport phenomena (phonon emission and transfer into the L valleys) can be investigated through the use of THETA devices. Ultimately, information gained this way should affect not only ballistic devices, but more conventional devices as well, and, more importantly, our understanding of the electronic properties of solids.

Acknowledgments

We wish to thank our collaborators, E. Calleja, W. P. Dumke, D. J. Frank, C. M. Knoedler, M. I. Nathan, L. Osterling, A. Palevski, U. Sivan, and M. V. Weckwerth. The continuous support of C. J. Kircher and E. J. Vanderveer throughout the various phases of this work is greatly appreciated. The work was partly supported by DARPA and was administered under Office of Naval Research Contract No. N00014-87-C-0709.

References

- 1. M. S. Shur and L. F. Eastman, *IEEE Trans. Electron Devices* ED-26, 1677 (1979).
- L. F. Eastman, R. Stall, D. Woodard, N. Dandekar, C. E. C. Wood, M. S. Shur, and K. Board, *Electron. Lett.* 16, 525 (1980).
- P. Hesto, J.-F. Pone, and R. Castagne, Appl. Phys. Lett. 40, 405 (1982).
- J. R. Hayes, A. F. J. Levi, and W. Wiegmann, Electron. Lett. 20, 851 (1984); Phys. Rev. Lett. 54, 1570 (1985).
- N. Yokoyama, K. Imamura, T. Ohshima, N. Nishi, S. Muto, K. Kondo, and S. Hivamizu. IEDM Tech. Digest, p. 532 (1984).
- 6. M. Heiblum, D. C. Thomas, C. M. Knoedler, and M. I. Nathan, Appl. Phys. Lett. 47, 1105 (1985).
- A. F. J. Levi, J. R. Hayes, P. M. Platzman, and W. Wiegmann, Phys. Rev. Lett. 55, 2071 (1985).
- M. Heiblum, M. I. Nathan, D. C. Thomas, and C. M. Knoedler, *Phys. Rev. Lett.* 55, 2200 (1985).
- M. Heiblum, I. M. Anderson, and C. M. Knoedler, Appl. Phys. Lett. 49, 207 (1986).
- M. Heiblum, K. Seo, H. P. Meier, and T. W. Hickmott, *Phys. Rev. Lett.* **60**, 828 (1988).
- 11. C. A. Mead. Proc. IRE 48, 359 (1960).
- J. M. Shannon, IEE J. Solid-State Electron Devices 3, 142 (1979).
- 13. M. Heiblum, Solid-State Electron. 24, 343 (1981).
- 14. J. M. Shannon and A. Gill, Electron. Lett. 17, 621 (1981).
- (a) R. J. Malik, K. Board, L. F. Eastman, D. J. Woodard, C. E. C. Wood, and T. R. AuCoin, *Proceedings of the Conference on Active Microwave Devices*, Cornell University, Ithaca, NY, 1981 (unpublished); (b) M. A. Hollis, S. C. Palmateer, L. F. Eastman, N. V. Dandekar, and P. M. Smith, *IEEE Electron Device Lett.* EDL-4, 440 (1983).
- I. Hase, H. Kawai, S. Imanaga, K. Kaneko, and N. Watanabe, Electron. Lett. 21, 757 (1985).
- 17. N. Yokoyama, K. Imamura, S. Muto, S. Hiyamizu, and H. Nishi, *Jpn. J. Appl. Phys.* 24, L853 (1985).
- A. P. Long, P. H. Beton, and M. J. Kelly, Semicond. Sci. Technol. 1, 63 (1986).
- U. K. Reddy, J. Chen, W. Kopp, C. K. Peng, D. Mui, and H. Morin, *IEEE Trans. Electron Devices* ED-33, 1865 (1986);
 U. K. Reddy, J. Chen, C. K. Peng, and H. Morkoç, *Appl. Phys. Lett.* 48, 1799 (1986).
- K. Imamura, S. Muto, T. Fujii, N. Yokoyama, S. Hiyamizu, and A. Shibatomi, *Electron. Lett.* 22, 1148 (1986).

- C. Y. Chang, Y. C. Liu, M. S. James, Y. H. Wang, S. Luryi, and S. Sze, IEEE Electron Device Lett. EDL-7, 497 (1986).
- M. Heiblum, M. V. Fischetti, W. P. Dumke, D. J. Frank, I. M. Anderson, C. M. Knoedler, and L. Osterling, *Phys. Rev. Lett.* 58, 816 (1987).
- F. Capasso, S. Sen, A. Y. Cho, and A. L. Hutchinson, *Appl. Phys. Lett.* **50**, 930 (1987).
- 24. A. Chandra and L. F. Eastman, *J. Appl. Phys.* **51**, 2669 (1980).
- A. F. J. Levi, J. R. Hayes, P. M. Platzman, and W. Weigman, *Phys. B* 134, 4801 (1985).
- M. Heiblum, D. Galbi, and M. V. Weckwerth, *Phys. Rev. Lett.* 62, 1057 (1989).
- M. E. Kim, A. Das, and S. D. Senturia, *Phys. Rev. B* 18, 6890 (1981).
- 28. R. Jalabert and S. Das Sarma, Phys. Rev. B. 41, 3651 (1990).
- M. Heiblum, E. Calleja, I. M. Anderson, W. P. Dumke, C. M. Knoedler, and L. Osterling, *Phys. Rev. Lett.* 56, 2854 (1986).
- I. Hase, H. Kawai, S. Imanaga, K. Kaneko, and W. Watanabe, Conference Proceedings, International Workshop on Future Electron Devices: Superlattice Devices, Japan, 1987, p. 63.
- 31. M. Chadrasekhar and F. H. Pollack, *Phys. Rev. B* **15**, 2127 (1970)
- S. Krishnamurthy, M. A. Berding, A. Sher, and A.-B. Chen, J. Appl. Phys. 63, 4540 (1989).
- K. Seo, M. Heiblum, C. M. Knoedler, W.-P. Hong, and P. Bhattacharya, Appl. Phys. Lett. 53, 1946 (1988).
- K. Seo, M. Heiblum, C. M. Knoedler, J. Oh, J. Pamulapati, and P. Bhattacharya, *IEEE Electron Device Lett.* 10, 73 (1989).
- P. Bhattacharya, *TEEE Electron Device Lett.* **10,** 73 (1989). 35. M. Büttiker and R. Landauer, *Phys. Rev.* **49,** 1739 (1982).
- A. Palevski, M. Heiblum, C. P. Umbach, C. M. Knoedler, A. N. Broers, and R. H. Koch, *Phys. Rev. Lett.* 62, 1776 (1989).
- S. Y. Chou, J. S. Harris, and R. F. W. Pease, *Appl. Phys. Lett.* 52, 1982 (1988).
- K. Ismail, D. A. Antonaidis, and H. I. Smith, *Appl. Phys. Lett.* 55, 598 (1989).
- A. Palevski, C. P. Umbach, and M. Heiblum, *Appl. Phys. Lett.* 55, 1421 (1989).

Received July 20, 1989; accepted for publication February 2,

Mordehai Heiblum IBM Research Division, Thomas J. Watson Research Center, P.O. Box 218, Yorktown Heights, New York 10598. Dr. Heiblum is a Research Staff Member and Manager of the Microstructure Physics group in the Logic, Memory, and Packaging Department. He received his B.S. degree from the Israel Institute of Technology (Technion) in 1973, his M.S. degree from Carnegie Mellon University in 1974, and his Ph.D. degree from the University of California at Berkeley in 1978—all in electrical engineering. In 1978 he joined IBM at the Thomas J. Watson Research Center, where he has worked on epitaxial crystal growth via molecular beam epitaxy, ballistic transport of hot carriers, and electric transport in nanostructures. In 1986 he received an IBM Outstanding Innovation Award for his work on the discovery of ballistic transport in semiconductors. Dr. Heiblum is a member of the American Physical Society and the Institute of Electrical and Electronics Engineers.

Massimo V. Fischetti IBM Research Division, Thomas J. Watson Research Center, P.O. Box 218, Yorktown Heights, New York 10598. Dr. Fischetti graduated from the University of Milan, Italy, in 1974 with a "Laurea" in physics. He received a Ph.D. degree in physics from the University of California, Santa Barbara, in 1978. Dr. Fischetti joined the Thomas J. Watson Research Center in 1983, after four years of experience in experimental solid-state physics at the Physics Laboratories of SGS-Thomson and 3M-Italy. He is currently a Research Staff Member in the Logic, Memory and Packaging Department. Dr. Fischetti has done experimental and theoretical work on the degradation of thin silicon dioxide films, and on the theory of electron transport in insulators. He has received two IBM Outstanding Innovation Awards, one in 1986 for the Monte Carlo simulation of electron transport in SiO₂ and one in 1989 for the creation of the DAMOCLES program. Since 1985, Dr. Fischetti has been working on the Monte Carlo modeling of electron transport in small semiconductor devices.